Marquette University
e-Publications@Marquette

Chemistry Faculty Research and Publications   Chemistry, Department of

Global Permutationally Invariant Potential Energy Surface for Ozone Forming Reaction

Mehdi Ayouz
Ecole Centrale de Paris

Dmitri Babikov
Marquette University, dmitri.babikov@marquette.edu

Global permutationally invariant potential energy surface for ozone forming reaction

Mehdi Ayouz[1,2] and Dmitri Babikov[1,a)]

[1]*Chemistry Department, Wehr Chemistry Building, Marquette University, Milwaukee, Wisconsin 53201-1881, USA*
[2]*Laboratoire de Génie des Procédés et Matériaux, Ecole Centrale de Paris, Bât. Dumas, 92295 Châtenay-Malabry Cedex, France*

We constructed new global potential energy surface for $O + O_2 \rightarrow O_3$ reaction. It is based on high level electronic structure theory calculations and employs fitting by permutationally invariant polynomial functions. This method of surface construction takes full advantage of permutation symmetry of three O nuclei and allows reducing dramatically the number of *ab initio* data points needed for accurate surface representation. New potential energy surface offers dramatic improvement over older surface of ozone in terms of dissociation energy and behavior along the minimum energy path. It can be used to refine the existing theories of ozone formation. © *2013 American Institute of Physics.* [http://dx.doi.org/10.1063/1.4799915]

I. INTRODUCTION

Fitting the potential energy surface by permutationally invariant polynomial functions[1] carries significant advantages, particularly for those molecules where several atoms are identical.[2–7] For the molecules where all atoms are identical (allotropes) this should be the method of choice.[8] It allows reducing significantly the number of *ab initio* data points needed for accurate surface representation, as well as automatically takes care of the intrinsic molecular symmetry. The resultant PES is analytic and smooth everywhere in the configuration space, free of any cusps (sharp artifacts, typical to other methods of surface representation such as splines). Gradients and Hessians of the potential energy function can also be computed analytically. While such fit is global, one can still emphasize the important regions of the PES. Adding new points to the existing PES is straightforward too.

One very important small homonuclear molecule is ozone, a triatomic molecule of oxygen, O_3. Its potential energy surface has been constructed in the past[9] using *ab initio* data at icMRCI+Q/cc-pVQZ level of theory with CASSCF(12,9) active space. That surface was represented by a 3D-spline of data points on a structured (rectangular) grid. Close to 6000 points total were used and the grid was quite dense near the bottom of the covalent well. The surface was claimed to be accurate at low energies,[10] but it contained several serious deficiencies at high energies.[11] First, the surface was way too shallow. For example, the dissociation energy of O_3 on that surface is 936 cm^{-1} smaller than a recent experimental value of 1.143 eV.[12] Predictions of vibrational spectra using the surface of such quality are questionable. Even the validity of predicted thermochemical data would be unreliable, since dissociation energy deviates from experimental

value by more than 10%. Second, that surface contained an artifact – a barrier along the minimum energy path (MEP) to dissociation.[13] The height of the barrier was only 47 cm^{-1} above the dissociation limit, but it was shown that the temperature dependence of the atom exchange rate is sensitive to this feature.[14] Experimental kinetics data suggest that the reaction path is barrier-less.[15,16]

There were several attempts to determine the level of theory required to compute a better surface for O_3. Higher level electronic structure calculations by several authors carried out along the minimum energy path[13,17,18] showed that top of the barrier is, indeed, below the dissociation limit, which transforms barrier into a "submerged reef." It was also suggested that the improvement to dissociation energy can be achieved by increasing the basis set size. However, calculations with basis sets larger than quadruple-ζ are computationally demanding, and those have never been attempted for the global PES of O_3.

We found it feasible[19] to construct new, improved potential energy surface for ozone forming reaction,

$$O(^3P) + O_2(^3\Sigma_g^-) \rightarrow O_3(\tilde{X}),$$
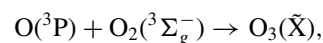
by combining (i) results of the high-level electronic structure theory calculations extrapolated to the complete basis set (CBS) limit and (ii) surface fitting by permutationally invariant polynomial functions. If we focus on the near-threshold part of the surface, relevant to thermal recombination kinetics, this method of fitting allows us to reduce the number of *ab initio* data points to roughly 500 which, in turn, makes the electronic structure calculations affordable.

In Sec. II of this paper we outline all equations needed to fit the PES of any homonuclear triatomic molecule using permutationally invariant polynomial functions and to construct analytic representations of its gradients and Hessians. In Sec. III this method is applied to fit new *ab initio* data for

---

a)Author to whom correspondence should be addressed. Electronic mail: dmitri.babikov@marquette.edu

the ground state PES of ozone. Major features of new PES are discussed and compared to those of the old surface for O_3. Conclusions are given in Sec. IV. Bohr units for distances will be used throughout the paper (1 Bohr = a_0 = 0.0529177 nm).

II. THEORETICAL FRAMEWORK

A. The fitting method

For a triatomic molecule with three identical atoms one useful set of the internal vibrational coordinates is a set of three positive inter-nuclear distances: $r_{ij} = \{r_{12}, r_{23}, r_{31}\}$. The indexes i and j label three possible pairs of oxygen atoms in O_3. The first step in fitting the PES is to introduce three *primitive* functions y_{ij} of the inter-nuclear distances r_{ij}. Since in O_3 all atoms are identical, the pairs of atoms are also identical. Thus, the three primitive functions y_{ij} are the same, just the arguments are different: $y_{12} = y(r_{12})$, $y_{23} = y(r_{23})$, and $y_{31} = y(r_{31})$. Analytic expression for $y(r)$ will be introduced later.

Next, the primitive functions y_{ij} are used to form various permutationally invariant polynomials. For any homonuclear triatomic molecule, including O_3, one can form the first order polynomial as

$$p_1 = y_{12} + y_{23} + y_{31}, \tag{1}$$

the second order polynomial as

$$p_2 = y_{12}y_{23} + y_{23}y_{31} + y_{31}y_{12}, \tag{2}$$

and the third order polynomial as

$$p_3 = y_{12}y_{23}y_{31}. \tag{3}$$

Note that each of these polynomials (p_1, p_2, and p_3) is a function of all three inter-nuclear distances in the molecule (r_{12}, r_{23}, and r_{31}) and, by construction, is a permutationally invariant function of these variables. The permutationally invariant polynomials of higher orders are obtained simply as products of p_1, p_2, and p_3.

At the final step, the permutationally invariant polynomials of various orders are used as basis functions for linear expansion of the potential energy surface $V_{fit}(r_{12}, r_{23}, r_{31})$. For example, including all expansion terms up to 5th order we can write the following analytic expression:

$$
\begin{aligned}
V_{fit} = & \; C_0 \cdot p_1^0 p_2^0 p_3^0 \\
& + C_1 \cdot p_1^1 p_2^0 p_3^0 \\
& + C_{2a} \cdot p_1^2 p_2^0 p_3^0 + C_{2b} \cdot p_1^0 p_2^1 p_3^0 \\
& + C_{3a} \cdot p_1^3 p_2^0 p_3^0 + C_{3b} \cdot p_1^1 p_2^1 p_3^0 + C_{3c} \cdot p_1^0 p_2^0 p_3^1 \\
& + C_{4a} \cdot p_1^4 p_2^0 p_3^0 + C_{4b} \cdot p_1^2 p_2^1 p_3^0 + C_{4c} \cdot p_1^1 p_2^0 p_3^1 \\
& + C_{4d} \cdot p_1^0 p_2^2 p_3^0 \\
& + C_{5a} \cdot p_1^5 p_2^0 p_3^0 + C_{5b} \cdot p_1^3 p_2^1 p_3^0 + C_{5c} \cdot p_1^2 p_2^0 p_3^1 \\
& + C_{5d} \cdot p_1^1 p_2^2 p_3^0 + C_{5e} \cdot p_1^0 p_2^1 p_3^1.
\end{aligned} \tag{4}
$$

Note that each basis function has a form of the product $p_1^{\ell_1} p_2^{\ell_2} p_3^{\ell_3}$, but the powers ℓ_1, ℓ_2, and ℓ_3 change from one basis function to another. The way in which the terms of Eq. (4)

are combined is quite clear – according to their order, j, given by the following simple expression:

$$j = \ell_1 + 2\ell_2 + 3\ell_3. \tag{5}$$

This also gives a natural method for truncating the expansion – according to the order of terms, j. The terms p_1^0, p_1^0, and p_3^0 are, of course, equal to unity but are included in Eq. (4) explicitly in order to emphasize a general structure of this expression.

For the purpose of convenience, the coefficients of linear expansion in Eq. (4) are labeled according to order j of the corresponding basis function. Thus, C_0 is coefficient of the zero-order function (which is just unity), C_1 is coefficient for the first-order function p_1, the doublet $\{C_{2a}, C_{2b}\}$ represents a set of coefficients for two possible functions of second order: p_1^2 and p_2, the triplet $\{C_{3a}, C_{3b}, C_{3c}\}$ represents a set of coefficients for three possible functions of third order: p_1^3, $p_1 p_2$, and p_3, and so on.

In order to fit the PES of ozone we used all terms of the permutationally invariant expansion up to 16th order. Such formula has $M = 204$ expansion coefficients to vary (including C_0) in order to achieve accurate fitting.[19] This is done automatically using the linear least squares fitting approach. Assume that the number of molecular geometries to fit is N (in this work the number of the *ab initio* data points was $N = 570$). A vector $\mathbf{V}$ of length N is introduced that contains the values of *ab initio* energies at these points. Another vector $\mathbf{V}_{fit}$ of length N is introduced that contains values of the fitting function at these points. We also introduce vector $\mathbf{C}$ of length M that contains a set of fitting coefficients. Finally, the matrix $\mathbf{A}$ of size $N \times M$ is introduced that allows obtaining values of the fit at the data points from the matrix-vector product:

$$\mathbf{V}_{fit} = \mathbf{AC}. \tag{6}$$

The structure of matrix $\mathbf{A}$ follows directly from Eq. (4). Namely, elements of the matrix $\mathbf{A}$ can be expressed as

$$A_{nm} = p_1^{\ell_1} p_2^{\ell_2} p_3^{\ell_3}, \tag{7}$$

where index n labels the data points and determines the values of p_1, p_2, and p_3 according to Eqs. (1)–(3), while index m labels the terms of expansion in Eq. (4) and defines a set of powers ℓ_1, ℓ_2, and ℓ_3. As introduced above: $1 \leq n \leq N$ and $1 \leq m \leq M$ (including C_0). Using this approach the elements of matrix $\mathbf{A}$ can be easily generated for any set of the data points and any order of the fitting function.

The goal of fitting is to minimize deviation between the fitting function and the *ab initio* energies at the data points:

$$\min \|\mathbf{V}_{fit} - \mathbf{V}\| = \min \|\mathbf{AC} - \mathbf{V}\|, \tag{8}$$

by finding the appropriate values of $\mathbf{C}$. In our numerical implementation this linear least squares fitting problem is solved using subroutine DGELS of LAPACK library.[20] A FORTRAN subroutine was developed to determine a set of adjustable coefficients $\mathbf{C}$ for any given set of N data points and any given order of the fitting function. This subroutine is general and can be used for any homonuclear triatomic molecule.

In our choice of the primitive function $y(r)$ we followed the work of Braams and Bowman[1] and employed the Morse

transform:

$$y = \exp\{-r/\lambda\}. \tag{9}$$

This function transforms the inter-nuclear distance r into the Morse variable y; λ is a fixed parameter that possesses units of length and depends on the system. Thus, $y_{ij} = \{y_{12}, y_{23}, y_{31}\}$ represents a set of Morse variables for the molecule under consideration. In the homo-nuclear molecules one value of λ can be used for all pairs or atoms. After several tries the value of $\lambda = 1.75\ a_0$ was chosen for ozone.

B. Analytic gradients and Hessians from the fit

Clearly, analytic expression of the PES should permit analytic computation of gradients and Hessian matrix. For the purposes of this section, it is more convenient to rewrite the expansion of Eq. (4) in the following formal way, where the expansion coefficients are labeled by one index m:

$$
\begin{aligned}
&V_{\text{fit}}(y_{12}, y_{23}, y_{31}) \\
&= \sum_{m=1}^{M} C^{(m)} p_1^{l_1^{(m)}} p_2^{l_2^{(m)}} p_3^{l_3^{(m)}} \\
&= \sum_{m=1}^{M} C^{(m)} (y_{12} + y_{23} + y_{31})^{l_1^{(m)}} \\
&\quad \times (y_{12} y_{23} + y_{23} y_{31} + y_{31} y_{12})^{l_2^{(m)}} (y_{12} y_{23} y_{31})^{l_3^{(m)}}. \tag{10}
\end{aligned}
$$

Note that here the sets of powers are also labeled by index m: $l_1^{(m)}$, $l_2^{(m)}$, and $l_3^{(m)}$. They are different for different terms of expansion, as it was explained in Sec. II A (see Eq. (5)).

The gradient of V_{fit} with respect to variable y_{ij} can be obtained from Eq. (10) by doing analytic differentiation by parts:

$$
\frac{\partial V_{\text{fit}}}{\partial y_{ij}} = \sum_{m=1}^{M} C^{(m)} \Big[l_1^{(m)} p_1^{l_1^{(m)}-1} p_2^{l_2^{(m)}} p_3^{l_3^{(m)}}
$$

$$
+ l_2^{(m)} (y_{ik} + y_{jk}) p_1^{l_1^{(m)}} p_2^{l_2^{(m)}-1} p_3^{l_3^{(m)}}
$$

$$
+ l_3^{(m)} y_{ik} y_{jk} p_1^{l_1^{(m)}} p_2^{l_2^{(m)}} p_3^{l_3^{(m)}-1} \Big]. \tag{11}
$$

Note that for every chosen pair of i and j, the value of k is such that $k \neq i$ and $k \neq j$. This expression can be conveniently re-written in the following concise form:

$$
\begin{aligned}
\frac{\partial V_{\text{fit}}}{\partial y_{ij}} &= \sum_{m=1}^{M} C^{(m)} p_1^{l_1^{(m)}} p_2^{l_2^{(m)}} p_3^{l_3^{(m)}} \\
&\quad \times \left[l_1^{(m)} \frac{1}{p_1} + l_2^{(m)} \frac{y_{ik} + y_{jk}}{p_2} + l_3^{(m)} \frac{y_{ik} y_{jk}}{p_3} \right]. \tag{12}
\end{aligned}
$$

Note that the product $C^{(m)} p_1^{l_1^{(m)}} p_2^{l_2^{(m)}} p_3^{l_3^{(m)}}$ in Eq. (12) is exactly equal to that in Eq. (10) for the potential. Thus, the only extra-effort required to compute analytic gradients is associated with computing a sum of three terms in the brackets of Eq. (12), for each variable y_{ij}.

The diagonal elements of the Hessian matrix are obtained by differentiating Eq. (12) with respect to y_{ij}. Again, the differentiation by parts is employed which, after some relatively straightforward but somewhat lengthy manipulations, leads to the following concise expression:

$$
\begin{aligned}
\frac{\partial^2 V_{\text{fit}}}{\partial y_{ij}^2} &= \sum_{m=1}^{M} C^{(m)} p_1^{l_1^{(m)}} p_2^{l_2^{(m)}} p_3^{l_3^{(m)}} \Big[l_1^{(m)} (l_1^{(m)} - 1) \frac{1}{p_1^2} \\
&+ l_2^{(m)} (l_2^{(m)} - 1) \frac{(y_{ik} + y_{jk})^2}{p_2^2} + l_3^{(m)} (l_3^{(m)} - 1) \frac{y_{ik}^2 y_{jk}^2}{p_3^2} \\
&+ l_1^{(m)} l_2^{(m)} \frac{2(y_{ik} + y_{jk})}{p_1 p_2} + l_1^{(m)} l_3^{(m)} \frac{2 y_{ik} y_{jk}}{p_1 p_3} \\
&+ l_2^{(m)} l_3^{(m)} \frac{2(y_{ik} + y_{jk}) y_{ik} y_{jk}}{p_2 p_3} \Big]. \tag{13}
\end{aligned}
$$

Similarly, the off-diagonal elements of the Hessian matrix are obtained by differentiating Eq. (12) with respect to y_{jk}. The result is

$$
\begin{aligned}
\frac{\partial^2 V_{\text{fit}}}{\partial y_{ij} \partial y_{jk}} &= \sum_{m=1}^{M} C^{(m)} p_1^{l_1^{(m)}} p_2^{l_2^{(m)}} p_3^{l_3^{(m)}} \Big[l_2^{(m)} \frac{1}{p_2} + l_3^{(m)} \frac{y_{ik}}{p_3} \\
&+ l_1^{(m)} (l_1^{(m)} - 1) \frac{1}{p_1^2} + l_2^{(m)} (l_2^{(m)} - 1) \frac{(y_{ij} + y_{ik})(y_{ik} + y_{jk})}{p_2^2} + l_3^{(m)} (l_3^{(m)} - 1) \frac{y_{ij} y_{ik}^2 y_{jk}}{p_3^2} \\
&+ l_1^{(m)} l_2^{(m)} \frac{y_{ij} + 2 y_{ik} + y_{jk}}{p_1 p_2} + l_1^{(m)} l_3^{(m)} \frac{y_{ik}(y_{ij} + y_{jk})}{p_1 p_3} + l_2^{(m)} l_3^{(m)} \frac{(y_{ij} + y_{ik}) y_{ik} y_{jk} + (y_{ik} + y_{jk}) y_{ij} y_{ik}}{p_2 p_3} \Big]. \tag{14}
\end{aligned}
$$

Again, the extra effort for getting analytic Hessians is associated with calculations of sums in the square brackets of Eqs. (13) and (14). The factors $C^{(m)} p_1^{l_1^{(m)}} p_2^{l_2^{(m)}} p_3^{l_3^{(m)}}$ can be re-used. It has to be noted that the off-diagonal terms of the Hessian matrix are symmetric:

$$
\frac{\partial^2 V_{\text{fit}}}{\partial y_{ij} \partial y_{jk}} = \frac{\partial^2 V_{\text{fit}}}{\partial y_{jk} \partial y_{ij}}. \tag{15}
$$

In order to obtain gradients and Hessians with respect to the inter-atomic distances r_{ij}, one can use the following transformations (assuming the dependence of Eq. (9)):

$$\frac{\partial V_{\text{fit}}}{\partial r_{ij}} = -\frac{1}{\lambda} e^{-r_{ij}/\lambda} \frac{\partial V_{\text{fit}}}{\partial y_{ij}}, \tag{16}$$

$$\frac{\partial^2 V_{\text{fit}}}{\partial r_{ij}^2} = \frac{1}{\lambda^2} e^{-r_{ij}/\lambda} \left(\frac{\partial V_{\text{fit}}}{\partial y_{ij}} + e^{-r_{ij}/\lambda} \frac{\partial^2 V_{\text{fit}}}{\partial y_{ij}^2} \right), \tag{17}$$

$$\frac{\partial^2 V_{\text{fit}}}{\partial r_{ij} \partial r_{jk}} = \frac{1}{\lambda^2} e^{-(r_{ij}+r_{jk})/\lambda} \frac{\partial^2 V_{\text{fit}}}{\partial y_{ij} \partial y_{jk}}. \tag{18}$$

Usually, the quantum dynamics methods (Schrödinger equation) require just the potential itself. The gradients are needed in the classical trajectory simulations. The Hessians are needed in the semi-classical initial value representation calculations.[21–23] Also, the gradients and/or Hessians are used by the energy minimization methods (for example, to determine the minimum energy path). It is very convenient to have all this information computed analytically, which provides accuracy and speed of calculations.

C. The *ab initio* calculations

All *ab initio* calculations were carried out using MOLPRO suite of the electronic structure theory codes.[24] The level of theory was icMR-CISD+Q using the CASSCF(12,9) active space. The relaxed version of Davidson cluster correction to energy was used. At each point of the PES we carried out two independent calculations: first with aug-cc-pVQZ and second with aug-cc-pV5Z basis sets. Then, for each point of the PES, we made extrapolation to the CBS limit using the following extrapolation formula:[17]

$$V_{\text{CBS}} = \frac{V_{\text{aug-cc-pVQZ}} \cdot 4^3 - V_{\text{aug-cc-pV5Z}} \cdot 5^3}{4^3 - 5^3}. \tag{19}$$

The value of dissociation energy obtained this way is in good agreement with the experiment (see Sec. III).

We also tried calculations with aug-cc-pV6Z basis sets and did two-point extrapolation based on the aug-cc-pV5Z and the aug-cc-pV6Z data. We found, however, that this adds only 3meV (about 24 cm^{-1}) to the dissociation energy of ozone and decided not to follow this path. We also tried calculations with larger active space CASSCF(18,12) but found that this level of theory overestimates dissociation energy. This indicates that larger active space should only be employed together with incorporation of the spin-orbit correction, which reduces dissociation energy by $\sim$80 cm^{-1}.[25] Such calculations would be extremely costly for the global PES of O + O$_2$ $\rightarrow$ O$_3$ reaction, so, we decided not to pursue them. We concluded that the CBS results of Eq. (19) with CASSCF(12,9) represent a reasonably accurate and affordable method of computing the PES of ozone.

A set of the *ab initio* data points used in the surface fitting contained only $N = 570$ points. This number of points is relatively small, taking into account that the PES of ozone is rather complicated (see Sec. III A) and that the *global* surface for the O + O$_2$ $\rightarrow$ O$_3$ reaction is constructed. This small set of the data points worked well because these points were not

arbitrary. Their positions in the configuration space have been pre-optimized prior to the *ab initio* calculations, using the old surface of ozone,[11] with the purpose of minimizing the RMS deviation of the fit, emphasizing the most important regions of the PES, and constructing an accurate PES based on a reasonably small set of points. All details of our pre-optimization procedure can be found in Ref. 19. Here we just want to mention that out of 570 points total only about 130 points were placed over the main (covalent) well of ozone. The remaining 440 points were placed in the region of the van der Waals well and near the "reef" that separates it from the main well. The overall RMS deviation of the fitting function from the data points was only 22 cm^{-1}, which is relatively small compared to the overall energy range of the surface (close to 10 800 cm^{-1}). The largest deviations were found in the high-energy repulsive parts of the PES, close to 0.2 eV above the dissociation limit. Near the bottom of the covalent well the deviations of the fit from the data points were about 3 cm^{-1}, near the top of the reef they were only about 2 cm^{-1}, and near the bottom of the vdW well the deviations were about 7 cm^{-1}. These data demonstrate excellent accuracy of the analytic representation of the PES.

D. The long-range behavior

The inter-nuclear distances r_{ij} and the Morse variables y_{ij} (used to construct the permutationally invariant fitting function) become inappropriate asymptotically, where the long-range interaction of O with O$_2$ defines the landscape of the PES. This long-range tail of the PES was fitted separately using a set of internal Jacoby coordinates $\{r, R, \gamma\}$ and the fitting function of the form

$$V_\infty(r, R, \gamma) = V_{\text{O}_2}(r) + V_{\text{O+O}_2}(R, \gamma) + V_0. \tag{20}$$

The first term in Eq. (20) is the Morse function used to describe the potential energy curve of O$_2$:

$$V_{\text{O}_2}(r) = D_{\text{O}_2} \cdot \left(\exp\left\{ -\frac{r - r_{\text{O}_2}}{\lambda_{\text{O}_2}} \right\} - 1 \right)^2. \tag{21}$$

Three fitting parameters: D_{O_2}, r_{O_2}, and λ_{O_2}, have their usual meaning. They were derived by fitting a one-dimensional slice of the PES along the inter-nuclear distance of O$_2$ (nine points in the range $2.10 < r < 2.46\ a_0$) and keeping the third O atom at a large distance: $R = 15.5\ a_0$, $\gamma = 117°$. The focus was on the low-energy part of the curve, near the bottom of O$_2$ well (below 0.2 eV). Here, we used the same level of the electronic structure theory as was used for calculations of the main part of the PES. The values of D_{O_2}, r_{O_2}, and λ_{O_2} derived in this way are given in Table I. The standard deviation of the 1D-fit of Eq. (29) from the *ab initio* data points was only 1.27 cm^{-1}.

The second term in Eq. (20) is

$$V_{\text{O+O}_2}(R, \gamma) = (C_5/R^5 + C_6/R^6) \cdot (1 + A \cdot \cos 2\gamma). \tag{22}$$

Here, the first R-dependent factor represents a multipole expansion of O + O$_2$ interaction. Namely, the term inversely proportional to R^5 describes the quadrupole-quadrupole interaction of O + O$_2$, while the term inversely proportional to R^6 describes interaction of the induced dipole of O with

TABLE I. Fitting parameters of the asymptotic part of the PES.

Fitting parameters (units)	Fitted values
r_{O_2} (a_0)	2.282664
λ_{O_2} (a_0)	0.762105
D_{O_2} (Hartree)	0.221509
C_5 (Hartree $\times a_0^5$)	–0.377947
C_6 (Hartree $\times a_0^6$)	–33.806438
V_0 (Hartree)	–225.199252

the induced dipole of O_2 (the dispersion interaction). Two fitting parameters in Eq. (22) are C_5 and C_6. They were derived by fitting a one-dimensional slice of the PES along the Jacoby coordinate R in the range $10 < R < 15.5 \, a_0$ (18 points), and keeping the other two coordinates fixed at $r = r_{O_2}$ and $\gamma = 117°$. Again, we used the same level of the electronic structure theory as was used for calculations of the main part of the PES. These *ab initio* data points and the resultant fit are presented in Fig. 1. We see that the data points in the asymptotic range are described very well by a simple analytic expression of Eq. (20). The standard deviation of this fit is only 0.015 cm^{-1}. The values of C_5 and C_6 obtained in this way are given in Table I.

The second γ-dependent factor in Eq. (22) qualitatively represents angular dependence of asymptotic interaction of O_2 and O (quadrupole-quadrupole and dispersion). The value of angular anisotropy parameter $A = 0.10$ in Eq. (22) was chosen to connect smoothly the asymptotic expansion of Eq. (20) to the inner part of the surface, namely, V_∞ to V_{fit}. The resultant angular anisotropy of the asymptotic part of the PES is rather weak. For example, at a distance $R \sim 10 \, a_0$ between O_2 and O, the energy difference of T-shaped configuration (higher energy) and collinear configuration (lower energy) is only 1.8 cm^{-1}.[26]

Finally, V_0 in Eq. (20) is the asymptotic value of the fitting function at $r = r_{O_2}$ and $R \rightarrow \infty$, used here to determine the dissociation limit (by extrapolation), i.e., the value of energy that corresponds to the infinitely separated $O + O_2$,

which also determines the dissociation energy of O_3. At the level of the electronic structure theory used in this work this asymptotic value of energy was determined to be $V_0 = -225.199252$ Hartree. It is also included in Table I. From Fig. 1 we see that the last point of the grid computed *ab initio* at $R = 15 \, a_0$ is only less than 1 cm^{-1} below the dissociation limit.

In order to ensure that the 3D fitting function $V_{fit}(r_{12}, r_{23}, r_{31})$ connects smoothly to the asymptotic fitting function $V_\infty(r, R, \gamma)$ we used the switching function of Jacoby coordinate R:

$$f(R) = \frac{1}{2} + \frac{1}{2}\tanh\left(2\frac{R - R_{sw}}{\Delta R}\right). \qquad (23)$$

This switching occurs in the vicinity of the point $R_{sw} = 7.60$ a_0. The switching length is controlled by $\Delta R = 1.20 \, a_0$. The global potential energy surface V is represented in the entire configuration space by the following combined expression:

$$V = V_{fit} \cdot [1 - f(R)] + V_\infty \cdot f(R) - V_0. \qquad (24)$$

The overall shift by the asymptotic value V_0 is for convenience to have the dissociation limit at $V = 0$.

III. RESULTS AND DISCUSSION

A. Global view of the PES

In order to emphasize the permutational invariance of the O_3 PES built in this work we use, for the graphical representation and analysis, the adiabatically adjusting hyper-spherical (APH) coordinates $\{\rho, \theta, \phi\}$ of the triatomic molecule.[27] In these coordinates, the permutation symmetry is described entirely by the hyper-angle ϕ, such that $0 < \phi < 2\pi$. The PES of a homonuclear triatomic molecule should exhibit the three-fold symmetry: it should be symmetric with respect to reflection through the $\phi = 0$, $\phi = 120°$, and $\phi = 240°$ planes (see Fig. 2(a)). Working with the APH coordinates, it is also useful to remember that the small-amplitude motion along the hyper-radius ρ correlates with the symmetric stretching normal mode, while the large-amplitude motion along ρ describes dissociation. Small-amplitude motion along ϕ correlates with the asymmetric stretching normal mode, while the large-amplitude motion along ϕ describes pseudo-rotation.[28] The hyper-angle θ correlates with the bending normal mode.

In Fig. 2 we show an iso-energy surface for the PES of ozone in three dimensions. In this approach to PES visualization the configuration space where the potential energy of the molecule is higher than a given cut-off value (here 0.1 eV above the dissociation threshold) is made transparent, while the configuration space classically accessible to the motion of nuclei at this energy is made visible as a 3D-structure. Such picture gives a global view of the PES in all three dimensions. Since there is no need to fix one of three variables, all features of the PES can be seen simultaneously. Two views of the iso-energy surface are given: Fig. 2(a) represents the frontal view, when the reader looks at the $\{\theta, \phi\}$-plane along the ρ-axis, while Fig. 2(b) shows the perspective view from a convenient angle. Of course, some effort is needed in order to understand

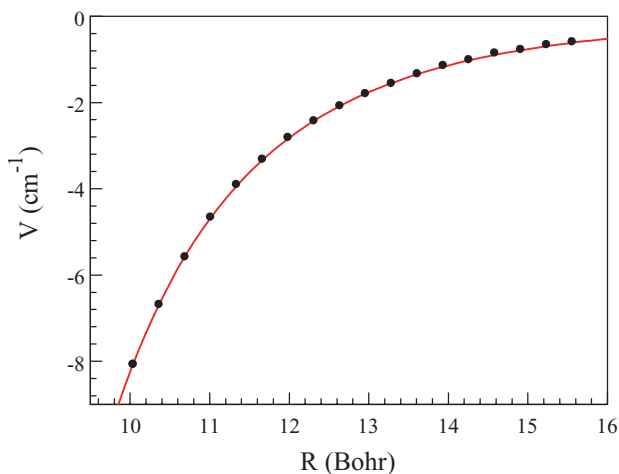FIG. 1. *Ab initio* data points (dots) and their analytic fit by Eq. (22) in the asymptotic region of $O + O_2$ potential. The other two coordinates are kept fixed at $r = 2.28 \, a_0$ and $\gamma = 117°$. Parameters of the fit are given in Table I.
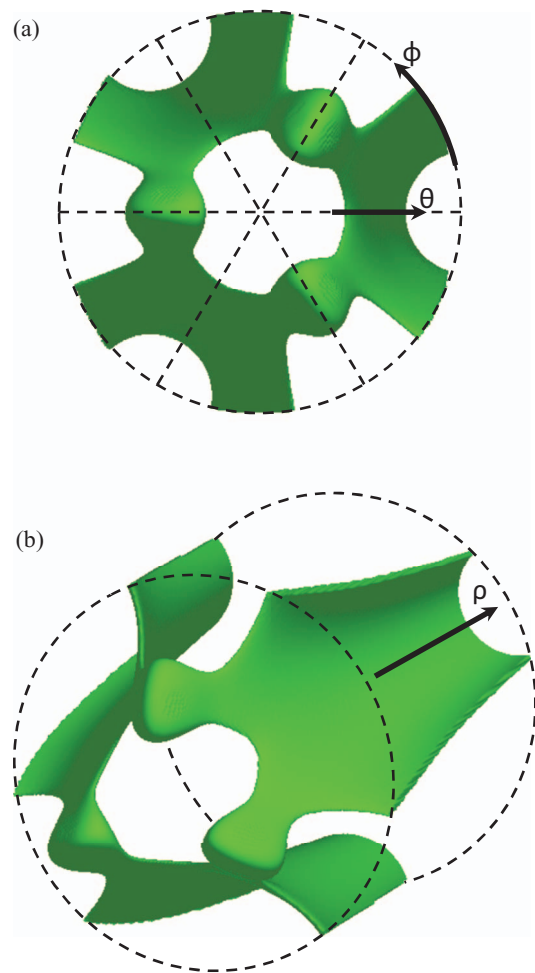
FIG. 2. Three-dimensional representation of the global PES of O_3 using the isoenergy surface in hyper-spherical coordinates. This surface confines the configuration space in $\{\rho, \theta, \phi\}$ accessible to the classical motion of nuclei at energy of 0.1 eV above the dissociation threshold. The "frontal" view (a) emphasizes permutation symmetry. Dashed circle corresponds to linear arrangement of three O nuclei. Dashed lines correspond to C_{2v} configurations. The "angular" view (b) demonstrated connection of three covalent wells at small ρ to three dissociation channels at large ρ.

the meaning of different parts of the 3D-structure in Fig. 2. It helps to remember that the motion of nuclei takes place inside the iso-energy surface, where the energy is lower than the cut-off value.

Figure 2 demonstrates several important concepts. First of all, the permutation symmetry of ozone is clearly seen. The three energetically identical covalent wells are observed in Fig. 2 as three ellipsoidal-like lobes at small values of ρ and near $\phi = 0$, $\phi = 120°$, and $\phi = 240°$. The three energetically identical dissociation channels are observed as semicircle-like structures at large values of ρ near $\phi = 60°$, $\phi = 180°$, and $\phi = 300°$. The overall structure of the PES is symmetric with respect to reflection through three planes that contain these six values of the hyper-angle ϕ.

Next, we see that each of the covalent wells is connected symmetrically to two dissociation channels, and each dissociation channel is symmetrically connected to two covalent wells. These features are related to the fact that O_3 can dissociate by releasing each of its two terminal atoms (going into

two different channels) and, similarly, when O atom collides with O_2 molecule it can attach to one or the other end of it (forming two different products). In Fig. 2 we can see six pathways that connect three covalent wells to three channels. They all are energetically equivalent, of course. We also can see that each such pathway goes through the narrow bottleneck, which represents the transition state, the "reef" structure (see Sec. III B).

Finally, Fig. 2 demonstrates the possibility of isomerization from one covalent well of ozone into two other wells. Such isomerization can happen only at high energies and requires crossing two "reefs": one bottleneck on the way out (of the initial) and second bottleneck on the way into (the final) covalent well. It is quite amazing that all these features of ozone PES can be seen on a single iso-energy surface in 3D. The only feature of O_3 PES that cannot really be seen clearly in Fig. 2 is the shallow van der Waals well (for each dissociation pathway, i.e., six of them for the entire configuration space). This is due to the relatively large value of the energy cut-off (0.1 eV) used in Fig. 2. If this value is reduced, the six van der Waals wells also become visible.

B. The MEP

Using analytic derivatives of the PES we carried out energy optimization in order to determine the minimum energy path for $O + O_2 \rightarrow O_3$ reaction and derive energies and geometries for critical points of the PES. The Newton-Raphson second-order minimization method was employed.

Figure 3 (green line) shows detailed view of the MEP in the high energy region, just below the dissociation threshold. The vdW well and the reef, which separates it from the covalent well, are clearly seen. The upper part of covalent well is also seen in the left part of Fig. 3. This behavior of the PES is consistent with earlier calculations by other authors.[13,17,18] Note, however, that those earlier calculations were carried out
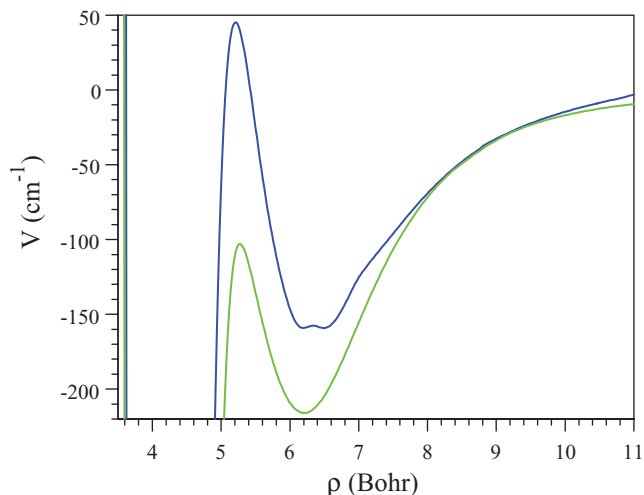

FIG. 3. Potential energy along the minimum energy path on the ozone PES in the vicinity of dissociation threshold. A deep covalent well (to the left), a shallow vdW well (to the right), as well as the "reef" structure between them are all clearly seen. Green – new global PES of this work. Blue – older PES of Ref. 9.

TABLE II. Critical points of the O_3 PES.

Quantity	r_1 (a_0)	r_2 (a_0)	α (deg)	ρ (a_0)	E (cm^{-1})
Covalent minimum	2.402	2.402	116.82	4.042	–9177.33
The "reef"	2.273	3.904	114.33	5.271	–102.96
vdW minimum	2.279	4.849	114.90	6.206	–216.02

along the minimum energy path only, while here we have a global 3D-PES. On our PES the vdW well is $\sim$ 216 cm^{-1} deep and the top of the reef is $\sim$ 103 cm^{-1} below the dissociation limit (see Table II). Recall that the previous global *ab initio* PES of O_3, from Schinke group,[9] had a serious deficiency. Instead of the "submerged" reef, that surface had a barrier of about 47 cm^{-1} above the dissociation threshold. The MEP for Schinke's surface is also shown in Fig. 3 (blue line). The most popular O_3 PES, still in use nowadays, was constructed by Babikov in Ref. 11, where he lowered the barrier into a reef, matching the results of higher-level calculations along the MEP.[13] This was done in a semi-empirical fashion, by adding the analytic correction function[11] to the PES of Schinke.[9] In the new global surface constructed here such correction is not needed anymore. The reef feature is reproduced *ab initio* and globally, in the entire configuration space.

The depth of covalent well on our PES is $\sim$9177 cm^{-1} (see Table II) which is only 42 cm^{-1} less than a recent experimental value of $D_e = 1.143$ eV.[12] Again, this property of our PES represents a dramatic improvement over the older PES of Schinke,[9] where the dissociation energy was 1.027 eV (which is 936 cm^{-1} less than a recent experimental value). Thus, in terms of the dissociation energy, new PES of ozone constructed here offers an improvement by a factor of more than 20. Accurate value of dissociation energy is needed not just for computing enthalpy of the ozone forming reaction but also in order to predict correctly the density of states near dissociation threshold, which is essential to understanding dynamics of the ozone formation process.[29]

An interesting feature of ozone MEP is demonstrated by Fig. 4. As we stretch the molecule, we see that initially the MEP follows bending motion, in which two O–O bonds remain equal. This makes sense, since the lowest frequency mode in ozone is bending, and the MEP should certainly follow excitation of this normal mode. However, in the asymptotic range the MEP should follow the local stretching mode (bond breaking), because it is impossible to dissociate O_3 by bending and would be very hard to do this by symmetric stretching of both bonds simultaneously. So, there should be a point on the PES where the MEP switches from the normal-mode bending motion to the local-mode stretching motion. This switch occurs suddenly, close to $\rho = 4.56\ a_0$ (see Fig. 4), when one of the O–O bonds quickly elongates while the other contracts. In fact, at this point the MEP splits onto two equivalent passes, each leading to a distinct dissociation channel. It seems to us that this property is general, and should occur on the global PESs of other molecules too.

We also found that the value of bending angle α changes very little along the MEP in O_3. As one goes through the
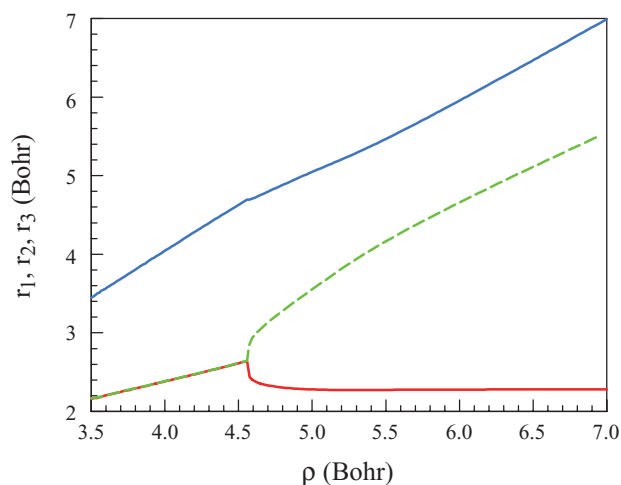

FIG. 4. Variation of inter-particle distances r_1 (red), r_2 (green), and r_3 (blue) in O_3 along the minimum energy path. This picture emphasized transition from the normal-mode behavior (at lower energies) to the local-mode behavior (at higher energies). At lower energies the molecule remains symmetric, $r_1 = r_2$. At $\rho \approx 4.57\ a_0$ this behavior changes abruptly to the asymmetric stretching motion with $r_1 < r_2$.

covalent well, the reef, and the vdW well (by stretching the bond) the variations of bending angle do not exceed 2.5° (see Table II). This interesting feature can be used to justify the dimensionally reduced models of ozone formation.[30,31]

C. Calculations of the bound states

In order to further quantify the new PES for O_3 we looked closer at the PES near the bottom of the covalent well. Using the method described below we computed energies of several low-lying vibrational eigenstates. For the purpose of comparison, we have also carried out the equivalent calculations for the older PES of ozone.[11] States of O_3 are characterized according to one of the irreducible representations $\Gamma = A'_1, A''_1, A'_2, A''_2, E'$, or E'' of the molecular symmetry group D_{3h}. In the case of $J = 0$, the vibrational states can be characterized in C_{3v} symmetry subgroup according to the irreducible representations A_1, A_2, and E.[32,33] The representation E is two-dimensional, whereby it has two degenerate states. At low levels of vibrational excitation, energies of E-states are indistinguishable from those of A_1 and A_2.

The energies and wave functions of vibrational states of non-rotating O_3 ($J = 0$) were computed using the APH coordinates and the sector-adiabatic coupled-channel technique.[32] In this approach, the full dimensional 3D Schrödinger equation for the vibrational motion is solved in two steps, which can be thought of as numerical "decoupling" of different degrees of freedom. First, the hyper-radius ρ is partitioned into a large number of sectors (intervals) and the two-dimensional angular part of the Schrödinger equation in (θ, ϕ) is solved numerically for each sector with $\rho = \rho_\xi$ fixed (as a parameter) at the center of each sector. The local 2D energies $E(\rho_\xi)$ and wave functions, the potential coupling matrices, and the overlap matrices between the adjacent sectors are also computed at this step. In the second step, a set of 1D coupled-channel equations is obtained for the hyper-radial coordinate

ρ and is solved using the propagation method. In this procedure, the coupling is recovered and accurate full dimensional solutions of the Schrödinger equation are obtained using the exact Hamiltonian and including all couplings of the PES.

The code of Brian Kendrick was used, that employs an efficient hybrid FBR/DVR algorithm[33] to solve the angular part of the problem in (θ, ϕ) and uses Numerov propagator for solving the coupled-channel equations in ρ. In our calculations, focused on the covalent well, a relatively short range of ρ values was treated: $3.55 \leq \rho \leq 5.25 \ a_0$ (just inside the "reef," see Fig. 3). This interval was partitioned onto 170 sectors, so that the step size along ρ was only $0.01 \ a_0$. The DVR of θ uses Jacoby polynomials; its size was $l_\theta = 127$, which gives the number of Gauss-Legendre quadrature points in the full range of θ. The FBR of ϕ uses complex exponential functions; the basis set size was $m_\phi = 148$. The energy cut-off value in the sequential diagonalization/truncation algorithm was ρ-dependent and varied in the range between 5.5 eV at small ρ and 2.1–2.4 eV over the well and above the reef. The number of coupled channels in ρ was 28 for symmetry A_1 and 22 for symmetry A_2. The 2D energies $E(\rho_\xi)$ of these states are given in Fig. 5. They cover the range up to the dissociation threshold. We found that this is quite sufficient for accurate calculations of the lower vibrational states in O_3. The overall convergence of energy eigenvalues up to 3000 cm^{-1} above the ground vibrational state was better than 1 cm^{-1}.

The computed vibrational spectrum of O_3 in the range from the ground state up to 3000 cm^{-1} contains 17 states. In this energy range, the MEP follows the bending motion, in which two O−O bonds remain equal (see Fig. 4). For this reason, it appears relevant to label the vibrational states in terms of the normal mode quantum numbers (v_1, v_2, v_3), in addition to Γ and $J = 0$. So, energies, symmetries, and the normal mode assignments of the low-lying vibrational

TABLE III. Lower part of the vibrational spectrum and comparison with older PES.[11]

State number	New PES E (cm^{-1})	Symmetry	Assignment (v_1, v_2, v_3)	Old PES E (cm^{-1})	Difference ΔE (cm^{-1})
1	0.0	A_1	(0, 0, 0)	0.0	0.0
2	698.6	A_1	(0, 1, 0)	698.5	0.1
3	1073.8	A_2	(0, 0, 1)	1043.9	29.9
4	1120.9	A_1	(1, 0, 0)	1101.9	19.0
5	1397.1	A_1	(0, 2, 0)	1394.4	2.8
6	1756.7	A_2	(0, 1, 1)	1726.0	30.7
7	1812.9	A_1	(1, 1, 0)	1792.6	20.5
8	2095.5	A_1	(0, 0, 2)	2060.6	34.9
9	2114.4	A_1	(0, 3, 0)	2088.8	26.3
10	2163.9	A_2	(1, 0, 1)	2111.3	52.6
11	2233.1	A_1	(2, 0, 0)	2199.0	34.1
12	2439.3	A_2	(0, 2, 1)	2405.1	34.5
13	2503.9	A_1	(1, 2, 0)	2481.8	22.8
14	2781.9	A_1	(0, 1, 2)	2726.5	55.6
15	2793.8	A_1	(0, 4, 0)	2782.8	13.6
16	2837.7	A_2	(1, 1, 1)	2783.5	54.5
17	2917.9	A_1	(2, 1, 0)	2882.1	36.3

states are given in Table III. The reference point is the energy of the ground vibrational state. For the new PES this value is 0.95428 eV below the dissociation threshold and it is 0.95190 eV below the dissociation threshold for the old PES of ozone.[11] The last column of Table III shows differences between the vibrational energies computed with old and new surfaces. The differences are not negligible. The best agreement is found for the lowest frequency bending mode (quantum number v_2). For this mode, the fundamentals on two surfaces are only 0.1 cm^{-1} different. The bending overtones are only 2.8 cm^{-1} different. For the other two modes the deviations are much more pronounced. Namely, for the asymmetric-stretch (v_3) and the symmetric-stretch (v_1) the deviations are close to 30 and 20 cm^{-1}, respectively. These differences add up in the combination states, leading to even larger deviations, above 50 cm^{-1} (e.g., states #10, 14, and 16 in Table III).

In order to better represent the difference between two surfaces we fitted the spectrum of 17 lower states using the standard Dunham expansion formula.[34] This expression characterizes the vibrational spectrum by a set of three frequencies (ω_1, ω_2, and ω_3), three intra-mode anharmonicities (Δ_1, Δ_2, and Δ_3), and three inter-mode anharmonicities (Δ_{12}, Δ_{23}, and Δ_{31}). Another advantage is that this representation is unbiased with respect to the energy reference. The resultant fitting parameters are given in Table IV for both new and old surfaces. We see that in terms of both harmonic frequency and anharmonicity a much better agreement between the two surfaces is found, again, for the bending mode (ω_2 and Δ_2). For two stretching modes the differences are more significant for both harmonic frequencies (ω_1 and ω_3) and anharmonicities (Δ_1 and Δ_3).

In general, one can think of two sources of observed frequency differences: First is the level of electronic structure theory (higher for new PES) and second is the method of surface representation (numerical spline vs. analytic fit). Recall
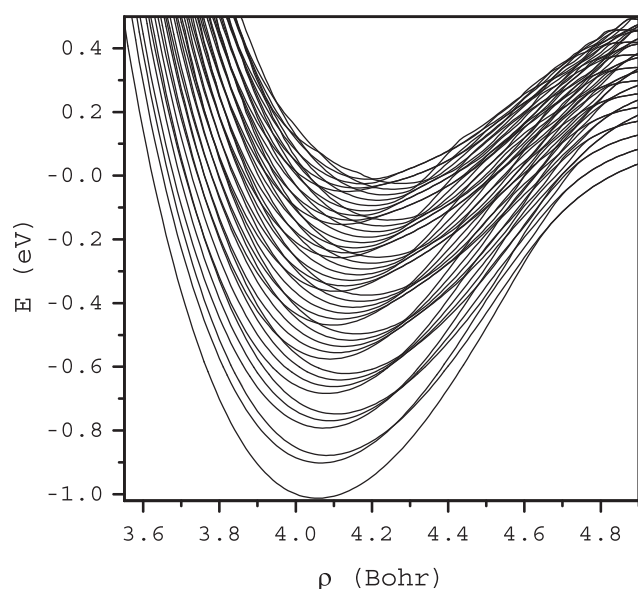

FIG. 5. Adiabatic surface-function energies for calculations of vibrational states in the covalent well of O_3 PES. Only the configuration space up to $\rho \approx 5 \ a_0$ and the energy range up to dissociation threshold $E = 0$ are covered. Both symmetries A_1 and A_2 are shown.

TABLE IV. Dunham fit of the vibrational spectrum and comparison with older PES.[11]

Fitting parameter (cm^{-1})	New PES	Old PES	Difference
ω_1	1148.7	1128.9	19.8
ω_2	717.0	711.6	5.4
ω_3	1127.4	1097.1	30.3
Δ_1	3.91	2.57	1.35
Δ_2	0.99	0.79	0.21
Δ_3	18.31	13.51	4.80
Δ_{12}	10.24	7.55	2.69
Δ_{23}	14.13	16.53	−2.39
Δ_{31}	28.37	35.72	−7.35
Standard deviation	7.20	4.64	2.56

that the RMS deviation of our fit is 22 cm^{-1} (see Sec. II). This is not much, particularly if one keeps in mind that this value characterizes the entire global surface of chemical reaction. However, our results suggest that fundamental frequencies may be affected by the fit. Indeed, during construction of this PES we put more emphasis on the "reef" region and the vdW well, relevant to the ozone forming reaction. The covalent well region, relevant to spectroscopy of stable ozone, was emphasized less. For example, out of 570 *ab initio* data points total, only about 50 points fall into the configuration space and energy window relevant to 17 vibrational states is analyzed in Tables III and IV. Increasing the number of points in this region of the PES should improve predictions of the fundamental frequencies. These additional calculations will be carried out in the near future. Importantly, the fitting method employed here allows easily adding new points to the PES, when they become available.

IV. CONCLUSIONS

New improved PES for the reaction that forms ozone was constructed by combining the method of surface fitting by permutationally invariant polynomial functions with *ab initio* calculations at icMR-CISD+Q level with CASSCF(12,9) active space and extrapolation of energies to the CBS limit. The advanced method of fitting allows reducing the number of points needed, while the high-level electronic structure theory provides accurate data.

Compared to the old surface of ozone, we dramatically improved the dissociation energy and reproduced *ab initio* (without any empirical adjustments) and globally (not just along the minimum energy path) the reef region of the PES. This new PES will be used to refine the existing models of ozone formation.[35, 36] It is available for download as supplementary material to this article.[37]

It is highly likely that new round of PES development will happen in the future, with the purpose of producing even more accurate PES. Recent calculations using dynamically weighted MRCI[38] indicate that the reef structure may transform into a "shoulder." This result is very interesting, but we have to note that it was obtained without incorporation of spin-orbit interaction. It is expected that spin-orbit splitting will lower the asymptotic value of energy for the ground state

PES, without affecting the interaction region (see Fig. 1 in Ref. 25). This may lead to re-appearance of the reef, although its final (actual) height may be somewhat smaller than what we have at the present level of theory.

The method of fitting the PES by permutationally invariant polynomial functions will always remain useful, even if newer *ab initio* data will replace the existing data, because it is very easy and fast (automatic) to refit the surface. This method is also general and can be applied to many other triatomic allotropes, such as S_3[39,40] or N_3.[28,41] For larger allotrops, such as S_4, N_4, or O_4, this method of fitting will probably be unsurpassed.

[1]B. J. Braams and J. M. Bowman, Int. Rev. Phys. Chem. **28**, 577 (2009).

[2]J. E. Mann, Z. Xie, J. D. Savee, J. M. Bowman, and R. Continetti, J. Chem. Phys. **130**, 041102 (2009).

[3]J. M. Bowman, B. J. Braams, S. Carter, C. Chen, G. Czakó, B. Fu, X. Huang, E. Kamarchik, A. R. Sharma, B. C. Shepler, Y. Wang, and Z. Xie, J. Phys. Chem. Lett. **1**, 1866 (2010).

[4]B. Fu, E. Kamarchik, and J. M. Bowman, J. Chem. Phys. **133**, 164306 (2010).

[5]Y. Wang, J. M. Bowman, and X. Huang, J. Chem. Phys. **133**, 111103 (2010).

[6]E. Kamarchik, L. Koziol, H. Reisler, J. M. Bowman, and A. I. Krylov, J. Phys. Chem. Lett. **1**, 3058 (2010).

[7]J. M. Bowman and B. C. Shepler, Annu. Rev. Phys. Chem. **62**, 531 (2011).

[8]Z. Xie, B. J. Braams, and J. M. Bowman, J. Chem. Phys. **122**, 224307 (2005).

[9]R. Siebert, R. Schinke, and M. Bittererová, Phys. Chem. Chem. Phys. **3**, 1795 (2001).

[10]R. Siebert, P. Fleurat-Lessard, R. Schinke, M. Bittererová, and S. C. Farantos, J. Chem. Phys. **116**, 9749 (2002).

[11]D. Babikov, B. Kendrick, R. B. Walker, R. T Pack, P. Fleurat-Lesard, and R. Schinke, J. Chem. Phys. **118**, 6298 (2003).

[12]B. Ruscic, Results obtained from active thermochemical tables (ATcT) based on the Core (Argonne) Thermochemical Network; version 1.110 (unpublished), see http://atct.anl.gov/Thermochemical%20Data/version%20Alpha%201.110/index.html.

[13]R. Hernández-Lamoneda, M. R. Salazar, and R. T Pack, Chem. Phys. Lett. **355**, 478 (2002).

[14]P. Fleurat-Lessard, S. Y. Grebenshchikov, R. Siebert, R. Schinke, and N. Halberstadt, J. Chem. Phys. **118**, 610 (2003).

[15]H. Hippler, R. Rahn, and J. Troe, J. Chem. Phys. **93**, 6560 (1990).

[16]M. R. Wiegell, N. W. Larsen, T. Pedersen, and H. Egsgaard, Int. J. Chem. Kinet. **29**, 745 (1997).

[17]R. Schinke and P. Fleurat-Lessard, J. Chem. Phys. **121**, 5789 (2004).

[18] F. Holka, P. G. Szaley, T. Muller, and V. G. Tyuterev, J. Phys. Chem. A **114**, 9927 (2010).

[19] M. Ayous and D. Babikov, Adv. Phys. Chem. **2012**, 951371 (2012).

[20] LAPACK, version 3.3.1, a freely available software package available from *Netlib* at http://www.netlib.org/lapack.

[21] E. Vetoshkin and D. Babikov, J. Chem. Phys. **125**, 024302 (2006).

[22] E. Vetoshkin and D. Babikov, Phys. Rev. Lett. **99**, 138301 (2007).

[23] E. Vetoshkin and D. Babikov, J. Chem. Phys. **127**, 154312 (2007).

[24] H.-J. Werner, P. J. Knowles, R. Lindh, F. R. Manby, M. Schütz *et al.*, MOLPRO, version 2009.1, a package of *ab initio* programs, 2009, see http://www.molpro.net .

[25] M. Tashiro and R. Schinke, J. Chem. Phys. **119**, 10186 (2003).

[26] M. Lepers, B. Bussery-Honvault, and O. Dulieu, J. Chem. Phys. **137**, 234305 (2012).

[27] D. Babikov, P. Zhang, and K. Morokuma, J. Chem. Phys. **121**, 6743 (2004).

[28] D. Babikov, B. Kendrick, P. Zhang, and K. Morokuma, J. Chem. Phys. **122**, 044315 (2005).

[29] D. Babikov, B. Kendrick, R. B. Walker, and R. T Pack, J. Chem. Phys. **119**, 2577 (2003).

[30] L. Jiang and D. Babikov, Chem. Phys. Lett. **474**, 273 (2009).

[31] M. Ivanov and D. Babikov, J. Chem. Phys. **134**, 174308 (2011).

[32] B. K. Kendrick, R. T Pack, R. B. Walker, and E. F. Hayes, J. Chem. Phys. **110**, 6673 (1999) and references therein.

[33] B. K. Kendrick and R. T Pack, J. Chem. Phys. **104**, 7475 (1996).

[34] L. Wang and D. Babikov, Phys. Rev. A **83**, 022305 (2011).

[35] M. Ivanov and D. Babikov, J. Chem. Phys. **136**, 184304 (2012).

[36] M. Ivanov and D. Babikov, "On molecular origin of mass-independent fractionation of oxygen isotopes in the ozone forming recombination reaction," Proc. Natl. Acad. Sci. U.S.A (published online), doi:10.1073/pnas.1215464110.

[37] See supplementary material at http://dx.doi.org/10.1063/1.4799915 for FORTRAN subroutines of the PES.

[38] R. Dawes, P. Lolur, J. Ma, and H. Guo, J. Chem. Phys. **135**, 081102 (2011).

[39] J. S. Francisco, J. R. Lyons, and I. H. Williams, J. Chem. Phys. **123**, 054302 (2005).

[40] K. A. Peterson, J. R. Lyons, and J. S. Francisco, J. Chem. Phys. **125**, 084314 (2006).

[41] D. Babikov and B. Kendrick, J. Chem. Phys. **133**, 174310 (2010).